Nuclear Instruments and Methods in Physics Research B 269 (2011) 2740–2744

Contents lists available at SciVerse ScienceDirect

Nuclear Instruments and Methods in Physics Research B

journal homepage: www.elsevier.com/locate/nimb

# 6 MeV electron irradiation effects on electrical properties of Al/$TiO_2$/*n*-Si MOS capacitors

P. Laha [a], S.S. Dahiwale [b], I. Banerjee [a], S.K. Pabi [c], D. Kimd [d], P.K. Barhai [a], V.N. Bhoraskar [b], S.K. Mahapatra [a,*]

[a] Department of Applied Physics, Birla Institute of Technology, Mesra, Ranchi 835215, India
[b] Department of Physics, University of Pune, Pune 411007, India
[c] Department of Metallurgical & Material Engineering, Indian Institute of Technology, Kharagpur 721302, India
[d] Department of Material Science and Engineering, Korea University, Seoul, Republic of Korea

ARTICLE INFO

*Article history:*
Received 17 May 2011
Received in revised form 29 July 2011
Available online 3 September 2011

*Keywords:*
MOS device
Electron irradiation
*C–V* measurement
Leakage current
$TiO_2$

ABSTRACT

The irradiation effects of 6 MeV electrons on the electrical properties of Al/$TiO_2$/*n*-Si metal–oxide–semiconductor capacitors have been investigated. Nine Al/$TiO_2$/*n*-Si capacitors were fabricated using radio frequency magnetron sputtering and divided into three groups. Groups were irradiated with 6 MeV electrons at 10, 20, and 30 kGy doses, respectively, keeping the dose rate ~1 kGy/min. The variations in the capacitance–voltage and leakage current–voltage characteristics, in addition to the electrical parameters, such as conductance ($G/\omega$), flat-band voltage, interface trap density and the surface charge density with electron dose were studied. The Poole–Frenkel coefficient of the MOS capacitors was determined from current–voltage characteristics. Possible mechanisms for the enhanced leakage current in the electron irradiated MOS capacitors are discussed.

© 2011 Elsevier B.V. All rights reserved.

## 1. Introduction

Metal–oxide–semiconductor (MOS) devices are commonly used in different types of space applications [1]. During the flight mission period, the electronic components mounted on a spacecraft are exposed to space radiation. Among other electronic devices, MOS devices are vulnerable even at relatively low doses of radiation such as electrons, protons, and heavy ions [1,2]. On exposure to these radiations, electron–hole pairs can be created in the devices, mainly near the oxide junction. The trapping of electrons or holes at or near the junction leads to the formation of interface states. The interface charge can therefore change the operational characteristics of the irradiated device, and in extreme cases to catastrophic failure [3,4]. Furthermore, this radiation can also cause the formation of local defects and charge trapping in the insulator, affecting the device leakage current [5,6]. This necessitates a systematic study of electron irradiation effects on the MOS capacitors, as well as development of radiation hardened MOS devices. Although, the effects of ionizing radiation on MOS devices have been studied extensively since the 1960s using electron beam irradiation [7], reports on irradiation effecting on electrical properties of the MOS capacitor are rather scarce. A few reports are available on the irradiation effects of electrons on Al/$TiO_2$/Si capacitors [8], but a systematic study is required to correlate the changes in the leakage current and device parameters with the radiation dose.

Conventionally, the oxide layer in MOS capacitors is made of $SiO_2$. However, in a high dose radiation environment, an oxide layer of $TiO_2$ is a better alternative. Electron irradiation increases $Ti^{3+}$ ions as compared to $Ti^{4+}$ ion at $TiO_2$/Si interfaces. This variation in the Ti ion valence is beneficial for the stability in the performance of a MOS capacitor [9]. The oxide layer in a radiation-hardened MOS device should have high dielectric constant and long-term thermal stability. Depending upon the synthesis and annealing processes, the dielectric constant of $TiO_2$ varies from 20 to 80. In addition, $TiO_2$ has relatively high bandgap energy of ~3.2 eV, and high melting point of ~1843 °C [10].

In this paper, Al/$TiO_2$/*n*-Si capacitors were fabricated using a RF reactive magnetron sputtering system. The capacitors were post irradiated with 6 MeV electrons at different doses; (a) zero (virgin), (b) 10 kGy, (c) 20 kGy, and (d) 30 kGy. The device parameters were estimated using *C–V* and $G/\omega$–*V* measurements, and the leakage current mechanism was proposed from the $\ln|J|$ vs. $\sqrt{E}$ plots. The effect of 6 MeV electron irradiation was found to cause permanent changes in the silicon crystallinity, interfacial dangling bonds, defects and charge trapping in the MOS capacitor. The flat band voltage of irradiated Al/$TiO_2$/*n*-Si capacitor has been compared with reported data.

## 2. Experimental details

For making MOS capacitors, silicon substrates, of size 10 mm × 10 mm × 0.5 mm, were obtained by cutting *n*-type wafers. These substrates were cleaned with deionized water and

* Corresponding author. Tel.: +91 651 2275444; fax: +91 651 2275401.
*E-mail address:* skmahapatra@bitmesra.ac.in (S.K. Mahapatra).

0168-583X/$ - see front matter © 2011 Elsevier B.V. All rights reserved.
doi:10.1016/j.nimb.2011.08.024

dried. Later, these substrates were also treated with the dilute HF acid, and rinsed with deionized water. All these silicon substrates were dried at room temperature and a RF magnetron sputtering system was used for coating thin films of aluminium and $TiO_2$ on the silicon substrates. The details of this RF magnetron sputtering deposition system, along with the vacuum pumps, etc. are given in [11]. For sputter coating two targets, one of titanium (99.99%), and other of aluminum (99.99%), each in the form of disc, having 50 mm diameter and 3 mm thickness, were clamped at the respective positions inside the chamber of the coating system.

After mounting a few Si substrates on the sample holder inside the deposition chamber, the system was evacuated to obtain a base pressure of $\sim 10^{-6}$ mbar. The titanium target and the aluminium targets were cleaned by sputtering using argon gas. Using mass flow controllers, argon and oxygen gases were inserted inside the chamber, at an equal flow rate of ~50 sccm, so that the working pressure of $\sim 5 \times 10^{-2}$ mbar could be maintained. For the deposition of thin films, the RF oscillator was switched onto provide power at a level ~100 Watts. Initially, using the titanium target, titanium oxide thin films of different thickness were deposited on silicon substrates, by varying sputtering period from 3 to 21 min, in a step of 3 min. The structure and the thickness of each titanium oxide film deposited on silicon substrates were studied by GIXRD and ellipsometry. From the plot of the film thickness and deposition time, the RF sputtering system could be calibrated. The GIXRD results confirmed that the deposited film had a $TiO_2$ structure. For a sputtering period of 15 min, the deposited film was found to be uniform $TiO_2$ of 100 nm thickness.

Later, using the aluminium target, a thin film of aluminium was deposited on each of the $TiO_2$ coatings, by keeping sputtering period of 7 min. For a sputtering period of 7 min, the deposited film was found to be uniform Al of 275 nm thickness. In this manner, Al/$TiO_2$/*n*-Si MOS capacitors were fabricated. The film growth process was controlled by the solid vapor transformation through heat released to the substrate undergoing heterogeneous nucleation [12]. All these laboratory made Al/$TiO_2$/*n*-Si MOS capacitors were characterized by (i) measuring the thicknesses of the oxide layer by a Spectroscopic Ellipsometer (Nano – View Inc., Korea; SEMG1000-VIS) (ii) studying the crystallographic structure by GIXRD (Model: PAN analytical X' Pertpro 3040/60) (iii) measuring *C–V* and $G/\omega$–*V* characteristics and $\tan\delta$ values at 500 kHz, using HP4284 LCR Meter, and (iv) measuring the *I–V* characteristics using 2410 Keithley Source meter.

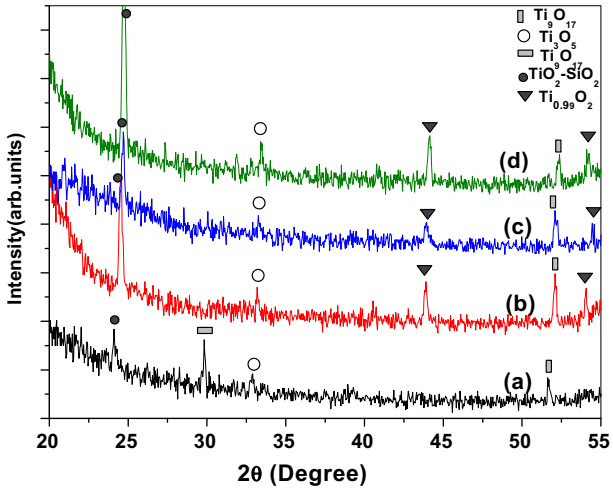


**Fig. 1.** GIXRD spectra of the $TiO_2$ thin-films deposited on silicon substrates, and irradiated with 6 MeV electrons different doses; (a) zero (virgin), (b) 10 kGy, (c) 20 kGy, and (d) 30 kGy.

A few characterized capacitors were divided into three groups, each consisting of five capacitors. These capacitors were irradiated with 6 MeV electrons, made available from the Race-Track Microtron of the University of Pune. The 6 MeV electrons beam, of pulse width ~1.6 μs, had diameter ~3 mm after exiting from the extraction window of the Microtron. The electron beam was therefore scattered by a thin tungsten foil, to cover the entire area ($10 \times 10$ mm$^2$) of the capacitor. For irradiation, one capacitor at a time was mounted on the Faraday cup, placed at a distance of ~150 mm away from the extraction port in air. The Faraday cup was connected to a current integrator for measuring the number of electrons falling on the capacitor. In this manner, each capacitor of the first group was irradiated with 6 MeV electrons to a dose of 10 kGy. Similarly, capacitors of the second and the third groups were irradiated with 6 MeV electrons to doses of 20 and 30 kGy, respectively. All the capacitors were irradiated at a constant dose rate ~1 kGy per minute. All the electron irradiated capacitors were also characterized following the same procedures as that adopted for the as-prepared capacitors.

## 3. Results and discussion

Fig. 1 shows the GIXRD spectra of $TiO_2$ films irradiated with 6 MeV electrons at different doses. Fig. 1(a) shows peaks at $2\theta = 23.67°$, 29.37°, 32.43°, and 51.19° corresponding to the plane (4 3 1) of $TiO_2$–$SiO_2$ (JCPDS card No. 84–1286), $(\bar{1}\,0\,1)$ of $Ti_9O_{17}$ (JCPDS card No. 85–1061), (0 2 3) of $Ti_3O_5$ (JCPDS card No. 89–4733) and $(2\,\bar{1}\,9)$ of $Ti_9O_{17}$ (JCPDS card No. 85–1061) respectively. The peak corresponding to $TiO_2$–$SiO_2$ signifies that $TiO_2$ molecules had diffused in silicon substrate on electron irradiation. Similarly, in Fig. 1, the peaks at $2\theta = 23.67°$, 32.43°, 44.05°, 54.34° and 51.19° corresponding to (i) (4 3 1) plane of $TiO_2$–$SiO_2$ [JCPDS card No. 84–1286], (ii) (0 2 3) plane of $Ti_3O_5$ [JCPDS card No. 89–4733)], (iii) (2 1 1) plane of $Ti_{0.99}O_2$ (JCPDS card No. 86–0148] and (iv) $(2\,\bar{1}\,9)$ plane of $Ti_9O_{17}$ [JCPDS card No. 85–1061], respectively. In addition, the peak at $2\theta = 44.05°$ corresponds to (2 1 0) plane of $Ti_{0.99}O_2$ [JCPDS card No. 86–0148].

The new peaks, corresponding to a high temperature rutile phase of $Ti_{0.99}O_2$ are also observed in the electron irradiated samples. The 6 MeV electrons transferred the energy to the lattice point causing local heating and generating a high temperature rutile phase. This energy is used for the rearrangement of the atoms. This also causes increase in the peak intensities as compared to the unirradiated sample. The signal of the $TiO_2$–$SiO_2$ peak indicates the diffusion process in the samples. The increase in the peak intensity with increasing electron dose implies occurrence of higher interdiffusion and recrystalization at the $TiO_2$–$SiO_2$ interface.

Fig.2 shows the measured *C–V* characteristics of Al/$TiO_2$/*n*-Si capacitor samples irradiated at different doses. It can be observed that the capacitance of all irradiated samples increases with increasing electron dose. This can be attributed to the variations in dielectric properties of the oxide layer, and charge trapping and generation of the dangling bonds at the $TiO_2$–Si interface. Moreover, due to an agglomeration process under electron irradiation, new grains can be produced from small crystallites, and grow until they completely consume the parent material which is involved in short range diffusion [13].

It is known that energetic electrons produce electron–hole pairs along the path in a semiconducting medium [14]. The number of electron–hole pairs increases with electron dose. The increase in charge density creates the Coulomb force which repels the charged atoms of the medium away from the atomic positions. A parallel shift of the depletion region in all the irradiated samples towards the negative voltage side with respect to electron dose was observed. This may be due to hole trapping at the vacancy sites of

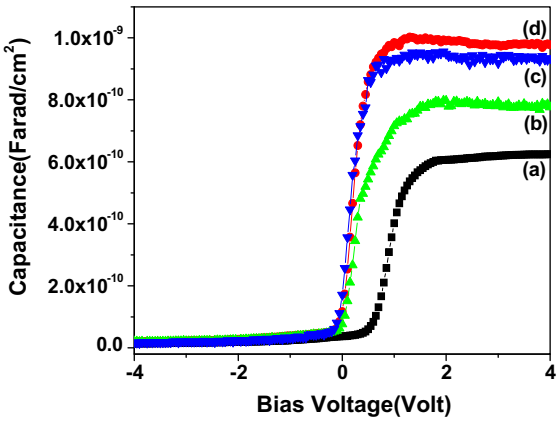


**Fig. 2.** C–V characteristics of the Al/$TiO_2$/*n*-Si MOS capacitors which were irradiated with 6 MeV electrons different doses; (a) zero (virgin), (b) 10 kGy, (c) 20 kGy, and (d) 30 kGy.

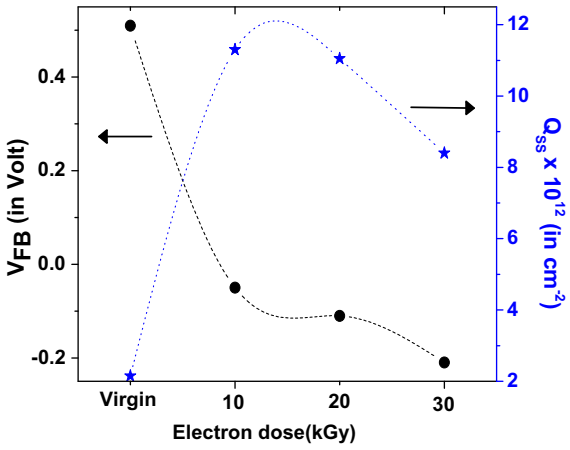


**Fig. 3.** Variations in the (i) flatband voltage ($V_{FB}$) and(ii) surface charge density ($Q_{SS}$) with the electron dose, for the Al/$TiO_2$/*n*-Si MOS capacitors,which were irradiated with 6 MeV electrons different doses; (a) zero (virgin), (b) 10 kGy, (c) 20 kGy, and (d) 30 kGy.

oxide layer. Increasing electron dose increases the number holes trapped at the vacancy sites.

Fig. 3 shows significant changes in flat band voltage ($V_{FB}$) and total charge density ($Q_{SS}$) of the electron irradiated samples. The values of the flat band capacitance, ($C_{FB}$), were calculated using the following relation:

$$C_{FB} = \frac{(C_{OX} \cdot C_{SFB})}{(C_{OX} + C_{SFB})} \quad (1)$$

where $C_{SFB}$ is the depletion layer capacitance, $C_{ox}$ is maximum value of the capacitance, and $C_{FB}$ is the capacitance value corresponding to the flat band voltage ($V_{FB}$). Fig. 3 shows that the flat band voltage decreases with increasing electron dose. Due to electron irradiation, the negative charged oxygen state, $O^-$, can be produced, which in turn transfers the titanium charge state $Ti^{4+}$ to $Ti^{3+}$ in the sample. These extra charges cause the shift of the flat band voltage $\Delta V_{FB}$ as well as depletion region. The number of electron–hole pairs produced in the sample increases with electron dose. This process leads to formation of more positive charge in the transition layer, thus causes shifting of the depletion region towards the negative voltage [15]. The flat band voltage of the irradiated Al/$TiO_2$/*n*-Si capacitors varied from 0.5 to −0.2 V, where as Liu et al. found the variations in flat band voltage of $TiO_2$ (10 nm)/*p*-Si from 0.2 to 1.3 V with the variations of electron dose [8].The total Charge Density ($Q_{SS}$), was calculated using the following expression;

$$Q_{SS} = \frac{C_{OX}}{A}|\phi_{MS} - V_{FB}| \quad (2)$$

where A is area of the capacitor sample, and $\phi_{MS}$ is the metal–semiconductor work function. Fig. 3 shows that $Q_{SS}$ initially increases, and then decreases with electron dose. Due to electron irradiation, the relative number of positive charges in the oxide layer increases over the initial fixed charges in the oxide layer before irradiation. The increased positive oxide charge is usually attributed to the oxygen-vacancy and dangling bonds [16].

The conductance at a frequency ~500 kHz, denoted $G/\omega$ at different voltages was also measured. Fig. 4 shows the $G/\omega$–$V$ characteristics of the Al/$TiO_2$/*n*-Si capacitor samples, irradiated with 6 MeV electrons at different doses. Fig. 4 shows that the conductance ($G/\omega$) increases with electron dose. Conductivity in oxides is governed mostly by the mechanism of hopping of the charge carriers. The number of sites available for hopping increases with electron dose. This enhances the mobility of charge carriers inside the irradiated MOS capacitor. As a result, the dielectric loss, which is associated with the probability of the electron transition, also increases with electron dose. Moreover, energetic electrons can also

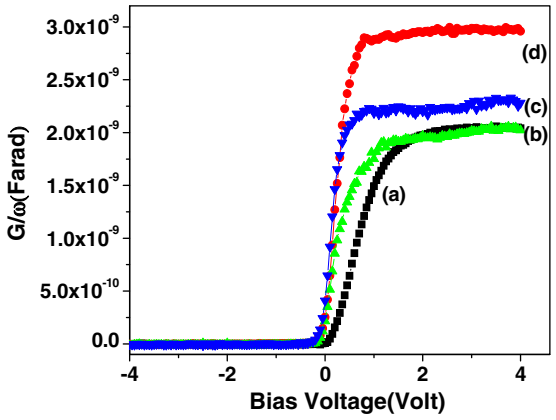


**Fig. 4.** $G/\omega$–$V$ characteristics of the Al/$TiO_2$/*n*-Si MOS capacitors which were irradiated with 6 MeV electrons at different doses; (a) zero (virgin), (b) 10 kGy, (c) 20 kGy, and (d) 30 kGy.

displace the lattice atoms and break the bonds. This process leads to formation of the dangling bonds and defects at the interface, which can help in recrystalization at the interface as well as in the oxide layer [17]. The variations in the degree of recrystallization, number of the dangling bonds and defects due to electron irradiation may vary the conductance properties of the MOS structure.

The interface trap density $D_{it}$ in the virgin and electron irradiated the Al/$TiO_2$/*n*-Si capacitors was estimated by the Hill–Coleman method [18]. Fig. 5 shows the interface trap density $D_{it}$, in the Al/$TiO_2$/*n*-Si capacitor samples irradiated with 6 MeV electrons at different doses. In a MOS capacitor, the oxide layer causes two types of interface layers, one with the top metal–oxide, and second with the oxide–Si substrate. These two interface layers are widely different due to the thermodynamic instability of these oxide materials with Si and metal. Generally, the oxide–silicon interface layer affects the Si channel mobility, while the defects at the metal–insulator interface cause the Fermi level pinning which affects the transistor drive current changes. Furthermore, $D_{it}$ also depends on the dangling bonds existing at the interface. In the present case, $D_{it}$ increases with electron dose which implies that the traps are created by irradiation [19]. The interfacial defects arise from the inter-diffusion atoms, vacancies and the dangling bonds. It is

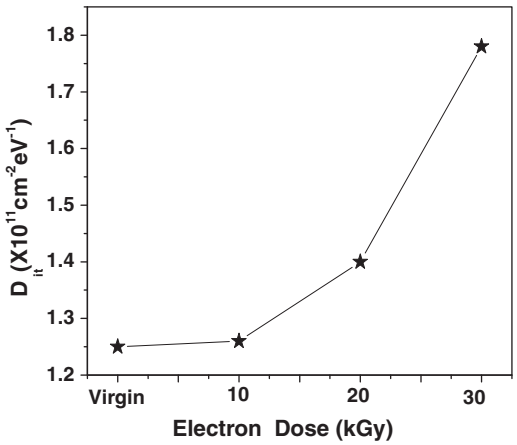


**Fig. 5.** Variation in the interface trap density, $D_{it}$, with the electron dose, for the Al/$TiO_2$/*n*-Si MOS capacitors,which were irradiated with 6 MeV electrons different doses; (a) zero (virgin), (b) 10 kGy, (c) 20 kGy, and (d) 30 kGy.

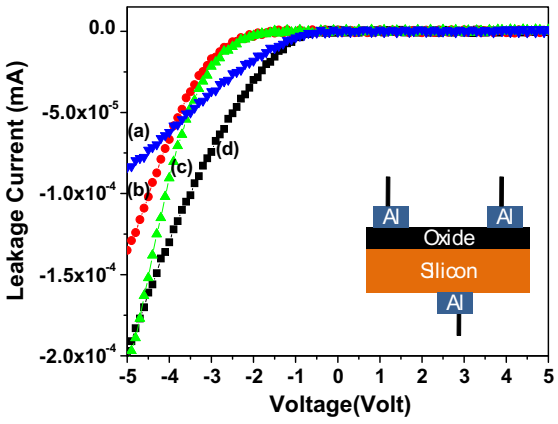


**Fig. 7.** Varaiation in the leakage cutrrent ($I$) with the voltage ($V$) for the Al/$TiO_2$/*n*-Si MOS capacitors, which were irradiated with 6 MeV electrons at different doses; (a) zero (virgin), (b) 10 kGy, (c) 20 kGy, and (d) 30 kGy.

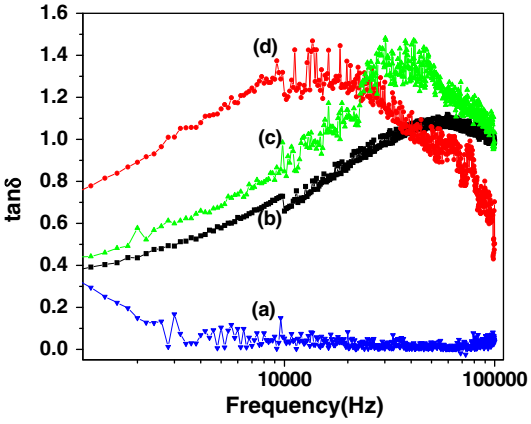


**Fig. 6.** Variation in the tan$\delta$ with the frequency for the of the Al/$TiO_2$/*n*-Si MOS capacitors which were irradiated with 6 MeV electrons at different doses; (a) zero (virgin), (b) 10 kGy, (c) 20 kGy, and (d) 30 kGy.

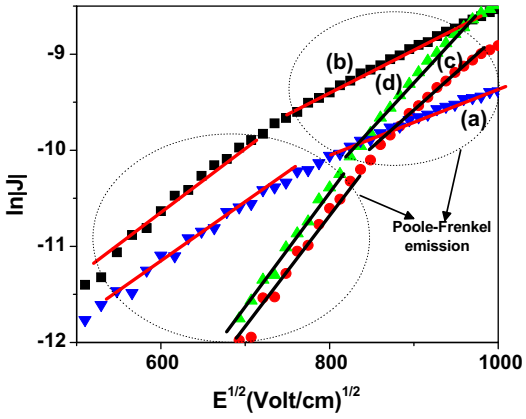


**Fig. 8.** Variations in ln|$J$| with $\sqrt{E}$ for the Al/$TiO_2$/*n*-Si capacitors irradiated with 6 MeV electrons at different doses; (a) zero (virgin), (b) 10 kGy, (c) 20 kGy, and (d) 30 kGy. The possible conductance mechanisms are shown by the dotted lines in the specified region.

expected that the dangling bonds increases with increasing electron dose because 6 MeV electron energy is sufficiently high to break Si–Si or Ti–O bonds, and form dangling bonds at the interface.

Generally, dipoles are produced in the oxide material, which governs the dielectric properties. This leads to dielectric relaxation, described by the following relation:

$$\tan\delta = \frac{2\pi f \tau_0 S_r}{1 + (2\pi f \tau_0)^2} \tag{3}$$

where tan$\delta$ is the dissipation factor, $S_r$ is the relaxation strength, which depends on the concentration of dipoles and the square of their dipole moments, $\tau_o$ is the relaxation time for the dipole orientation, and $f$ is the frequency of the applied electric field.

The dielectric relaxation characteristics of the MOS capacitors were studied from plot of the tan$\delta$ vs. log($f$), at a given temperature, $T$. Fig. 6 shows the tan$\delta$ vs. frequency in the range of 1 Hz to 100 kHz for the capacitors irradiated at different doses. In Fig. 6, there is no peak in the plot of the virgin capacitor sample at room temperture. This might be due to oscillations of the rigid molecules of the oxide material, under an applied oscillating electric field. In the spectra of the irradiated capacitor samples, the relaxation loss peak is observed. The width of the peak depends on the dielectric relaxation period, $\tau$, and therefore the observed broad peak can be attributed to the overlapping of a large number of different relaxation periods of the dipoles. Furthermore, Fig. 6 shows that in all the electron-irradiated capacitors, the dielectric loss increases with electron dose [20]. Moreover, the peak in the spectrum shifts gradually towards the lower frequency, as the electron dose increases. Following the relationship,($\omega \cdot \tau_o \cdot T \sim 1$), applicable to the dielectric loss peak, the shift in the relaxation loss peak to a lower frequency indicates that the relaxation period increases with increasing electron dose, without any significant change in the magnitude. The presence of a large number of the dangling bonds can also change the frequency response. At lower frequency these dangling bonds are more active than at the higher frequency, and therefore, a hump in the plot is observed in the low frequency region.

The appearance of a peak in the plots is due to matching of hopping frequency with the frequency of the external electric field. This is popularly known by interfacial polarization as established by the Koops and Maxwell–Wagner models [21–23]. Furthermore, the peak in the plot for the sample irradiated at high dose correlates to the resonance behavior which might be due to the interfacial polarization effects as well as due to the defects in the capacitor.

Fig. 7 shows the variation in the leakage current ($I$) with the voltage ($V$) for the samples irradiated at different doses. Fig. 7 shows that there is no variation in the leakage current at the

**Table 1**
The comparison of theoretical and experimental values of $\beta$.

| MOS capacitor | Theoretical (β) (eV $m^{1/2}$ $V^{-1/2}$) | | Experimental (β) (eV $m^{1/2}$ $V^{-1/2}$) | |
|---|---|---|---|---|
| | $\beta_{SC}$ | $\beta_{PF}$ | Low field | High field |
| (a) Al/$TiO_2$/*n*-Si (zero) virgin | $0.38 \times 10^{-5}$ | $0.76 \times 10^{-5}$ | $1.58 \times 10^{-5}$ | $0.87 \times 10^{-5}$ |
| (b) Al/$TiO_2$/*n*-Si irradiated at 10 kGy $e^-$ doses | $0.32 \times 10^{-5}$ | $0.64 \times 10^{-5}$ | $1.77 \times 10^{-5}$ | $1.13 \times 10^{-5}$ |
| (c) Al/$TiO_2$/*n*-Si irradiated at 20 kGy $e^-$ doses | $0.29 \times 10^{-5}$ | $0.58 \times 10^{-5}$ | $3.08 \times 10^{-5}$ | $2.09 \times 10^{-5}$ |
| (d) Al/$TiO_2$/*n*-Si irradiated at 30 kGy $e^-$ doses | $0.28 \times 10^{-5}$ | $0.56 \times 10^{-5}$ | $3.25 \times 10^{-5}$ | $2.73 \times 10^{-5}$ |

positive bias voltage, where the leakage currents changes when negative bias voltage is applied. The threshold voltage corresponds to the initiation of current decrease with increasing dose. The measured threshold voltages for leakage current are −1, −2, −3.5, and −4 V for the capacitors irradiated at different doses. Fig. 7 shows no identifiable trend in the behavior of the leakage current with dose, implying that the excited traps have only a minor effect on current. However, there is a significant change in threshold voltage for the leakage current. For high doses, some radiation-induced superfluous titanium brings extra energy states to the Si surface as a result of formation of extra energy states. The extra energy state exchanges electrons with the Fermi level, and produces an extra current, when the voltage is applied. It is very difficult to accurately establish the carrier flow mechanisms in MOS capacitors since leakage current is very sensitive due to the presence of local non-uniformities, such as non-uniform thickness, distribution of defects, the presence of small sized local micro defects related to the metal electrode area, etc. [24].The possible mechanism of leakage current has been explored through the following Frenkel–Poole expression;

$$J = J_0 \exp[(\beta_{PF}E^{1/2} - \phi_{PF})/K_B T] \quad (4)$$

where slope $= \frac{\beta_{PF}}{K_B T}$, $\beta_{PF} = 20 \times \beta_{SC}$, $\beta_{SC}$ is the Schottky coefficient, $\varphi$ is the barrier height, $J_0$ is the low-field current density, $K_B$ is the Boltzmann's constant, and $T$ is temperature (K).

The plots are showing variations of $\ln|J|$ with $\sqrt{E}$ for the Al/$TiO_2$/*n*-Si capacitor samples irradiated at different doses are shown in Fig. 8. This shows that the behavior of $\ln|J|$ vs. $\sqrt{E}$ is linear. The slopes were used for estimating the experimental values of "$\beta_{PF}$" using the expression-($K_B T \times$ slope). These experimental values of $\beta_{PF}$ were compared with corresponding theoretical values [10], given in Table 1. A comparison between the theoretical and the experimental values of $\beta_{PF}$ show that the leakage current of the virgin and the electron irradiated MOS capacitors are due to Frenkel–Poole type mechanism. The leakage current mechanism is depends on the film parameters, such as thickness, area, density, oxide material, etc. In our earlier publication (oxide layer thickness >50 nm), it was proposed that Schottky and Poole–Frenkel effects contribute to the leakage current, at for low and high field, respectively [10]. In the present work, it is observed that only the Poole–Frenkel mechanism is responsible for the leakage current in the oxide film of thickness ~100 nm. At the low values of the applied field, the electrons do not have enough energy to overcome the potential barrier, and therefore the Schottky type mechanism cannot contribute to the leakage current. In Frenkel–Poole mechanism, the electrons can tunnel the barrier and are transported through the traps in band gap of the insulator. The trap assisted conduction is highly probable at low fields. However, at high fields, the barrier height is reduced due to the combined effects of the image field and the Coulomb field. In the presence of positively charged trap levels, the conduction is possible through the conduction band.

## 4. Conclusions

Laboratory-made Al/$TiO_2$/*n*-Si capacitors were irradiated with 6 MeV electrons, at three doses. The variations in the electrical parameters, such as leakage current, conductance, flat-band voltage, interface trap density, and surface charge density of the MOS capacitor with the electron dose were studied. It was found that the electron beam causes variations in the crystallinity, generation of defects, leakage current and the number of the dangling bonds at the interface, which ultimately change the electrical properties. The results indicate that the electrical parameters of such a MOS capacitor can be tailored by energetic electron beam irradiation method.

## Acknowledgement

The authors wish to thanks to BRNS, D.A.E., Mumbai, (India) for the financial support under the research project.

## References

[1] F.A.S. Soliman, A.S.S. Al-Kabbani, K.A.A. Sharshar, M.S.I. Rageh, Appl. Radiat. Isot. 46 (5) (1995) 355–361.
[2] K.H. Zaininger, A.G. Holmes-Siedle, RCA Rev. 28 (1967) 208–240.
[3] P.F. Schmidt, M.J. Rand, J.P. Mitchell, J.D. Ashner, IEEE Trans. Nucl. Sci. Ns-16 (1969) 211–219.
[4] J.R. Cricchi, D.F. Barbe, Appl. Phys. Lett. 19 (1971) 49–51.
[5] M. Badila, Ph. Godignon, J. Millan, S. Berberich, G. Brezeanu, Microelectron Reliab 41 (2001) 1015–1018.
[6] H. García, S. Dueñas, H. Castán, A. Gómez, L. Bailón, R. Barquero, K. Kukli, M. Ritala, M. Leskelä, J. Vac, Sci. Technol. B 27 (1) (2009) 416–420.
[7] P.S. Winokur, J.R. Schank, P.J. Mcwhorter, P.V. Dressendorfer, D.C. Turpin, IEEE. Trans. Nucl. Sci. Ns-31 (1984) 1453.
[8] Chengshi Liu, Dengxue Wu, Lili Zhao, Zhijun Liao, Nucl Instrum Meth Phys Res B 268 (2010) 1446–1449.
[9] J.D. Zhang, S. Fung, Lin Li-Bin, Liao Zhi-Jun, Surf Coat Technol 158–159 (2002) 238–241.
[10] K.J. Hubbard, D.G. Schlom, J. Mater. Res. 11 (1996) 2757–2776.
[11] Pinaki Laha, A.B. Panda, S. Dahiwale, K. Date, K.R. Patil, P.K. Barhai, A.K. Das, I. Banerjee , S.K. Mahapatra, Thin Solid Films 519 (2010) 1530–1535.
[12] C. Merckling, M. El-Kazzi, L. Becerra, L. Largeau, G. Patriarche, G. Saint-Girons, G. Hollinger, Microelectron. Eng. 84 (2007) 2243–2246.
[13] W.D. Callister, Jr., David G. Rethwisch, R. Balasubramanium, Mater. Sci. Eng. (Wiley India (P) Ltd.) (2009).
[14] A. Tataroğlu, M.H. Bölükdemir, G. Tanır, S. Altındal, M.M. Bülbül, Nucl Instrum Meth Phys Res B 254 (2007) 273–277.
[15] F. Belgin Ergin, Raşit Turan, Sergiu T. Shishiyanu, Ercan Yilmaz, Nucl. Instrum. Meth. Phys. Res. B 268 (2010) 1482–1485.
[16] P. Thangadurai, W.D. Kaplan, V. Mikhelashvili, G. Eisenstein, Microelectron. Reliab. 49 (2009) 716–720.
[17] A. Tataroğlu, Ş. Altındal, M.H. Bölükdemir, G. Tanır, Nucl. Instrum. Meth. Phys. Res. B 264 (2007) 73–78.
[18] W.A. Hill, C.C. Coleman, Solid-State Electron. 23 (9) (1980) 987.
[19] A. Tataroğlu, M.H. Bölükdemir, G. Tanır, Ş. Altındal, M.M. Bülbül, Nucl. Instrum. Meth. Phys. Res. B 254 (2007) 273–277.
[20] P.S. Alegaonkar, V.N. Bhoraskar, P. Balaya, P.S. Goyal, Appl. Phys. Lett. 80 (4) (2002).
[21] J.C. Maxwell, Electricity and Magnetism, vol. 1, Oxford University Press, Oxford, 1929.
[22] K.W. Wagner, Ann. Phys. 40 (1913) 817.
[23] C.G. Koops, Phys. Rev. 83 (1951) 121.
[24] V. Mikhelashvili, P. Thangadurai, W.D. Kaplan, G. Eisenstein, Microelectron. Eng. 87 (2010) 1728–1734.